SCIENCE CHINA
Chemistry

•ARTICLES•
SPECIAL TOPIC: Photovoltaics

July 2019 Vol.62 No.7: 851–858
https://doi.org/10.1007/s11426-018-9430-8

Breaking 12% efficiency in flexible organic solar cells by using a composite electrode

Guang Zeng[1,4], Jingwen Zhang[1], Xiaobin Chen[1], Hongwei Gu[2], Yaowen Li[1*] & Yongfang Li[1,3]

[1]*Laboratory of Advanced Optoelectronic Materials, College of Chemistry, Chemical Engineering and Materials Science, Soochow University, Suzhou 215123, China;*
[2]*College of Chemistry, Chemical Engineering and Materials Science, Soochow University, Suzhou 215123, China;*
[3]*Beijing National Laboratory for Molecular Sciences, Institute of Chemistry, Chinese Academy of Sciences, Beijing 100190, China;*
[4]*College of Materials Science and Engineering, Nanchang Hangkong University, Nanchang 330063, China*

Received December 23, 2018; accepted January 23, 2019; published online March 18, 2019

The performance of flexible organic solar cells (OSCs) significantly relies on the quality of transparent flexible electrode. Here, we used silver nanowires (AgNWs) with various weight ratios to dope high-conductive poly(3,4-ethylenedioxythiophene): polystyrene sulfonate (PH1000) to optimize the optical and electronic properties of PH1000 film. A high-quality flexible composite electrode PET/Ag-mesh/PH1000:AgNWs-20 with smooth surface, a low sheet resistance of 6 Ω/sq and a high transmittance of 86% at 550-nm wavelength was obtained by doping 20 wt% AgNWs to PH1000 (PH1000:AgNWs-20). The flexible OSCs based on the PET/Ag-mesh/PH1000:AgNWs-20 electrode delivered a power conversion efficiency (PCE) of 12.07% with an open circuit voltage (V_{oc}) of 0.826 V, a short-circuit current density (J_{sc}) of 20.90 mA/cm^2 and a fill factor (FF) of 69.87%, which is the highest reported PCE for the flexible indium-tin oxide (ITO)-free OSCs. This work demonstrated that the flexible composite electrodes of PET/Ag-mesh/PH1000:AgNWs are promising alternatives for the conventional PET/ITO electrode, and open a new avenue for developing high-performance flexible transparent electrode for optoelectronic devices.

flexible electrodes, flexible organic solar cells, silver nanowire, composite electrode, power conversion efficiency

Citation: Zeng G, Zhang J, Chen X, Gu H, Li Y, Li Y. Breaking 12% efficiency in flexible organic solar cells by using a composite electrode. *Sci China Chem*, 2019, 62: 851–858, https://doi.org/10.1007/s11426-018-9430-8

1 Introduction

Organic solar cells (OSCs) have attracted more and more attention due to their intrinsic low-cost, lightweight and capability to be fabricated into semitransparent and flexible devices [1–7]. Especially, their flexibility is the most distinguished characteristic in comparison with the silicon, perovskite and other thin film based solar cells [8,9]. However, the flexible OSCs are still lag behind their rigid counterparts in power conversion efficiency (PCEs). A limitation of the PCEs is the quality of flexible electrodes. A high performance flexible electrode should possess the following characteristics: excellent mechanical flexibility, low sheet resistance, high transmittance in visible light range as well as excellent thermal stability [10]. Among the various candidates, indium tin oxides (ITO) based flexible electrodes have been commercialized and widely used in various flexible electronic devices [11]. However, its high cost, poor chemical properties, high sheet resistance and low mechanical stability hinder its applications for high performance flexible devices. Recently, silver nanowires (AgNWs) [12,13], silver grids [14], ultrathin metal [15], conducting polymers, such as poly(3,4-ethylenedioxythiophene):polystyrene sulfonate (PEDOT:PSS) [16,17] and carbon-based

*Corresponding author (email: ywli@suda.edu.cn)

materials [18] have been exploited as the alternatives of ITO. The performance of flexible OSCs in terms of PCE and mechanical stability have also made significant progress [19–23].

PEDOT:PSS is one of the most promising candidates as flexible electrodes, owing to its adjustable electronic properties, intrinsic flexibility and solution processability [24]. For example, doping polar organic molecules in aqueous PEDOT:PSS solution and film post treatment can boost the conductivity as high as 3000 S/cm [25–28]. Unfortunately, their low transmittances, corrosive treatment processes and hygroscopicity nature still limit their further applications, particularly in flexible OSCs. In comparison, AgNWs-based electrode exhibits higher conductivity and transmittance [29]. More importantly, the solution-processed AgNWs is adaptable to roll-to-roll processes for high throughput production. However, AgNWs electrodes still face the challenges of synthesizing high-quality AgNWs, constructing network structure, reducing junction resistance and controlling surface roughness [30]. In 2009, Ag grid that precisely patterned on a flexible substrate was developed, and was demonstrated to have high transmittance, excellent bending and stretching durability [14]. Recently, we utilized nanoprinting technology to construct a high-resolution and embedded Ag mesh on polyethylene terephthalate (PET) substrate (PET/Ag-mesh), where the Ag lines with a width of ~3 μm and a coverage of ~4%. When further combining it with dimethyl sulfoxide (DMSO) doped high-conductive PEDOT:PSS (D-PH1000), the resulting hybrid electrode PET/Ag-mesh/D-PH1000 showed a sheet resistance of 3–8 Ω/sq and an average visible transmittance (AVT) of around 80% [31,32]. Excitingly, the flexible OSCs based on this PET/Ag-mesh/D-PH1000 electrode realized a PCE of over 10% and exhibited robust bending durability [33]. Even though, there are still some bottlenecks hindering its development in terms of efficiency and large-scale processing: (1) unfavorable electronic contact between interface layer and active layer; (2) low transmittance of PH1000 film at a high conductivity.

In this work, we take the advantages of high-transmittance and high-conductive AgNWs to optimize the optical and electronic properties of PH1000, then combining with the PET/Ag-mesh substrate to construct a flexible composite electrode PET/Ag-mesh/PH1000:AgNWs. When doping 20 wt% of AgNWs into PH1000 solution (PH1000:AgNWs-20), the obtained flexible composite electrode PET/Ag-mesh/PH1000:AgNWs-20 showed a sheet resistance as low as 6 Ω/sq and high transmittance of 86% at 550 nm wavelength. More importantly, its root-mean-square surface roughness (RMS) can be reduced to 8.62 nm. When selecting PBDB-T-2F:IT-4F as active layer [34,35], the flexible OSCs with a device structure of PET/Ag-mesh/PH1000:AgNWs-20/PEIE/AZO (Al doped ZnO)/PBDB-T-2F:IT-4F/MoO_3/Al (Figure 1(a)) realized a record high PCE of 12.07% of the flexible OSCs, which is also higher than that of control device based on PET/Ag-mesh/PH1000 electrodes (PCE=11.12%). The promising photovoltaic performance was demonstrated to be attributed to the high-quality flexible electrodes with high transparency, high conductivity and favorable ohmic contact with active layer.

2 Experimental

2.1 Materials and method

Methanol, ethanol, 2-methoxyethanol and chlorobenzene (99% super dry J&K Seal) were purchased from J&K (China). Clevios PH1000 was purchased from Heraeus (Germany). Ag nanowires (AgNWs, aqueous solution, 0.5 wt%) solution was provided by Gu`s Nanotechnology (Zhejiang) Co., Ltd. (China). Polyethylenimine, 80% ethoxylated (PEIE, M_w=70000 g/mol), dissolved in H_2O with a concentration of 35 wt%–40 wt%, 1,8-diiodoctane (DIO) and zinc acetate dihydrate ($Zn(CH_3COO)_2$•$2H_2O$, 98%) were purchased from Sigma-Aldrich (USA). Aluminum nitrate

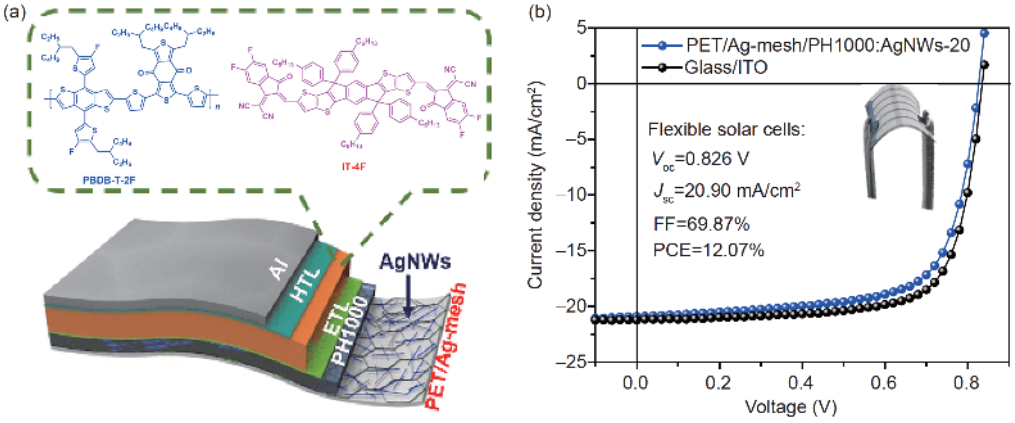

Figure 1 (a) Schematic of flexible OSCs with the structure of PET/Ag-mesh/PH1000:AgNWs/PEIE/AZO/PBDB-T-2F:IT-4F/MoO_3/Al; (b) *J-V* characteristics of the flexible devices based on PET/Ag-mesh/PH1000:AgNWs-20 and Glass/ITO electrodes (inset is photo image of corresponding flexible OSCs) (color online).

($Al(NO_3)_3$•$9H_2O$, 99.99%) was purchased from Aladdin (China). PBDB-T-2F and IT-4F were purchased from Organtecsolar Materials Inc (China). All of the materials were used without further purification. The PET/Ag-mesh flexible substrates were provided by Shine Optoelectronics (Kunshan) Co., Ltd. (China) [31]. The AZO was synthesized according to the literature [36].

2.2 Characterization

The transmittance and absorption spectra were measured using an Ultraviolet Spectrometer (Agilent Technologies Cary 5000 UV-Vis-NIR, USA). Film thickness was measured by a Profilometer D-100 (KLA-Tencor, USA). The sheet resistance was measured by a 4-Point Probes Resistivity Measurement System (Probes Tech RTS-9, China). All the scanning electron microscope (SEM) images were collected from a Hitachi SU8010 (Japan). The atomic force microscopy (AFM) images were obtained on an Bruker Nanoscope V atomic force microscope (Germany). Current density-voltage (*J-V*) characteristics of the devices were measured with a computer-controlled Keithley 2400 Source Measure Unit (USA) under the illumination of AM 1.5G (100 mW/cm^2) using a SS-F5-3A solar simulator (AAA grade, 50 mm×50 mm photobeam size) of Enli Technology Co., Ltd. (China). A 2 cm×2 cm monocrystalline silicon reference cell (SRC-00019) was purchased from Enli Technology CO., Ltd. (China). Photoluminence (PL) spectra were recorded from a FLS980 spectrofluorometer (Edinburgh Instruments, UK).

2.3 Composite electrodes fabrication

The 0.5-wt% AgNWs aqueous solution was concentrated to 1 wt% by centrifugation. The PH1000 was filtered to 1-wt% by a 0.45 μm filter before use. Then, the 1-wt% AgNWs solution was simply blended with the filtered PH1000 (0.45 μm filter) by various volume ratios of 1:9, 1:4 and 1:1, giving the corresponding weight ratios (AgNWs:PH1000) of 10% (PH1000:AgNWs-10), 20% (PH1000:AgNWs-20) and 50% (PH1000:AgNWs-50), respectively. Then the blend solution was stirred over 6 h to obtain a well dispersed mixture. The resulting mixtures were spin-coated onto the PET/Ag-mesh substrates that have already treated by plasma with air atmosphere. Consequently, they were thermally annealed at 120 °C for 15 min, and formed PET/Ag-mesh/PH1000:AgNWs composite electrodes. The thickness of PH1000:AgNWs films were controlled to be ~100 nm by tuning the spin-coating speed.

2.4 Device fabrication

PEIE/Al doped ZnO (PEIE/AZO) was selected as the electron transporting layer (ETL). Firstly, the PEIE solution (0.5% in 2-methoxyethanol) was spin-coated onto PET/Ag-mesh/PH1000:AgNWs electrode at 5000 r/min for 30 s. Then AZO solution was spin-coated onto the obtained PEIE film at 2000 r/min for 1 min, and followed by a thermal annealing process in air at 120 °C for 20 min. It should be noted that the PEIE was used to tune the work function of PH1000:AgNWs film for matching with that of AZO [37,38]. Then it was transferred into a N_2-filled glovebox, immediately. The active layer was deposited onto the AZO film by spin-coating PBDB-T-2F:IT-4F (10 wt%:10 wt%, 20 mg/mL) precursor solution at 1600 r/min for 60 s, where the chlorobenzene (CB) was selected as solvent and doped with 1-vol% DIO. The thickness of resulting PBDB-T-2F:IT-4F active layer is around 100 nm. MoO_3 (10 nm) and Al (100 nm) were sequentially deposited on the active layer by vacuum evaporation under 3×10^{-4} Pa. The effective area of each cell is 10 mm^2.

3 Results and discussion

3.1 Conductive and optical properties

Conductivity is one of the most important parameters for the electrode applied in OSCs. We firstly investigated the influence of AgNWs contents on their conductive properties, where the PH1000:AgNWs blend films were deposited on glass substrates with the same thickness of ~100 nm. It should be noted that the thicknesses of PH1000:AgNWs-50 and pure AgNWs films have a 10-nm fluctuation around 100 nm due to the poor film-forming ability of AgNWs. As shown in Figure 2(a), with increasing the AgNWs doping ratios from 0% to 100%, the conductivity was greatly increased from 3.53 to 2358 S/cm, accompanying with reduced sheet resistances from 2.83×10^4 to 43 Ω/sq. The significantly improved conductive properties suggest that the AgNWs can uniformly dispersed in both PH1000 solution and water, and the AgNWs in the solid state films can provide additional paths for charge transportation. When implanting the PH1000:AgNWs film onto the PET/Ag-mesh substrate, the resulting flexible composite electrodes PET/Ag-mesh/PH1000:AgNWs showed further substantially reduced sheet resistance. As shown in Figure 2(b), the composite flexible electrodes with weight ratios of 20% and 50% showed sheet resistances below 6 Ω/sq. When further doping with 5 wt% DMSO and 1 vol‰ fluorosurfactant Zonyl-FS300 (Zonyl), it can be reduced to 2.8 Ω/sq for the flexible electrode containing 20 wt% AgNWs. Such a low sheet resistance will be favorable of their application in large-area flexible OSCs.

We then investigated the optical properties of the flexible electrodes. As shown in Figure 2(c), after coating PH1000 onto the PET/Ag-mesh substrate, the hybrid PET/Ag-mesh/PH1000 shows a dramatically decreased transmittance in the

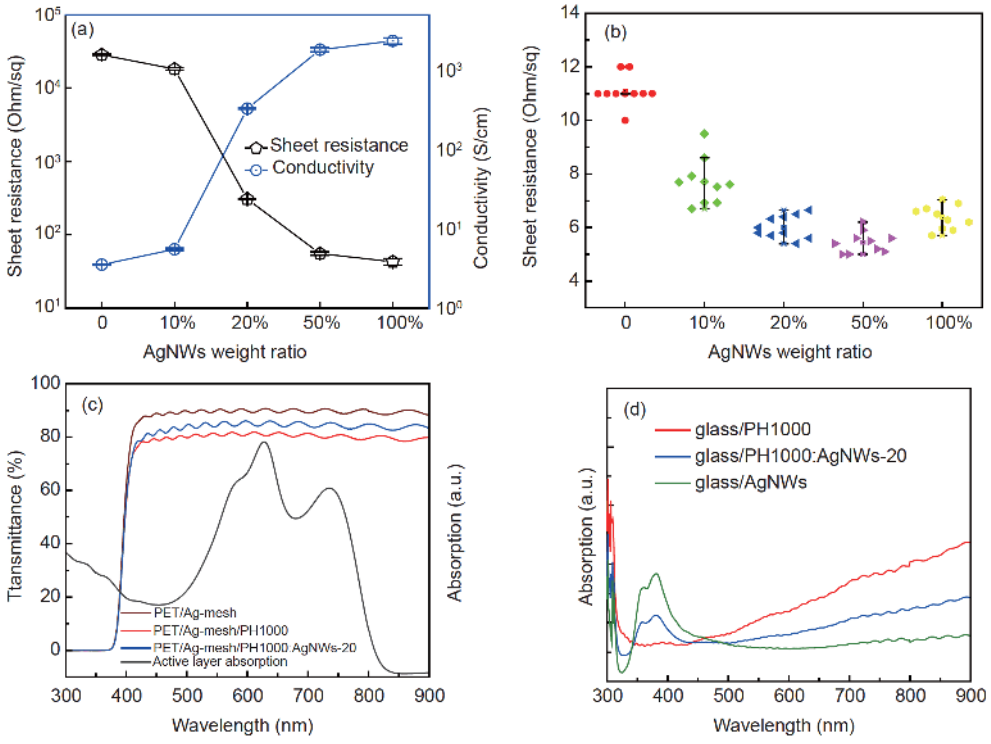

Figure 2 (a) Sheet resistance and conductivity variation of PH1000 film (on glass substrate) containing different AgNWs doping ratios. (b) Sheet resistance statistics of the PET/Ag-mesh/PH1000:AgNWs electrodes with different AgNWs doping ratios. (c) Transmittance of flexible electrodes: PET/Ag-mesh, PET/Ag-mesh/PH1000 and PET/Ag-mesh/PH1000:AgNWs-20%. The black line is the absorption spectrum of active layer PBDB-T-2F:IT-4F. (d) Absorbance of different conductive films of PH1000, AgNWs-20% and AgNWs, all the samples are fabricated on glass substrates (color online).

visible region, from ~91% to ~81% at the wavelength of 550 nm. It indicates that a high parasitic absorption accrued in 100-nm-PH1000 film. Although the pure AgNWs coated PET/Ag-mesh can avoid the parasitic absorption, the poor film-forming ability of AgNWs solution could lead to a rough surface due to the long AgNWs (10–18 μm) [10,13]. Interestingly, by doping AgNWs in PH1000, the transmittance of composite electrodes could be gradually increased from 81% to 88% (Figure S1, Supporting Information online). Particularly for the PET/Ag-mesh/PH1000:AgNWs-20%, 20-wt% AgNWs can be homogeneously deposited on PET/Ag-mesh and also significantly improve the transmittance (at 550 nm) to 86%, which is consistent with its reduced absorption intensity in the visible region (Figure 2(d)). The 5%-enhanced transmittance could be attributed to the light scattering and plasmonic effect of AgNWs that can be confirmed by the appearance of broad surface plasmon resonance (SPR) band in the UV region (Figure 2(d)) [29,39]. It is likely that the reduced PH1000 contents could also contribute to the transmittance to a certain degree due to the reduced parasitic absorption. Because the composition of the mixed film have been changed after incorporating AgNWs. With increasing the AgNWs content, the relative content of PH1000 will be decreased, which can reduce the intrinsic absorption of PH1000 in the long-wavelength region. In comparison, the AgNWs film has a weak absorption in this region. In addition, the enhanced transmittance region is consistent with the absorption spectrum of active layer PBDB-T-2F:IT-4F (Figure 2(c)), which would obviously enhance the photocurrent generation of the resulting OSCs [40,41].

3.2 Morphological characterization

The morphology of electrode plays an important role in the subsequent active layer growth, particularly for the flexible solar cells. Morphology evolution of various flexible electrodes was carried out by SEM (Figure 3(a–e)) and AFM (Figure 3(f–j)). As seen from SEM images, the AgNWs possess long length (10–18 μm) and short diameter (30 nm). Such large aspect ratio is very easy to form network structure without aggregation, which is evidenced from a strong broad absorption band that is absent in the bulk spectra (Figure 2 (d)) [42]. Meanwhile, the AgNWs network structure can well explain the increased transmittance and conductivity of PH1000:AgNWs blend films as mentioned above. AFM images (Figure 3(k–o)) were used to reveal the surface roughness of the flexible electrodes. As for the PET/Ag-mesh/PH1000, an extremely low RMS of 1.90 nm can be obtained. However, after incorporating the AgNWs in PH1000 film, the RMS values were obviously increased because the AgNWs are likely to penetrate through the

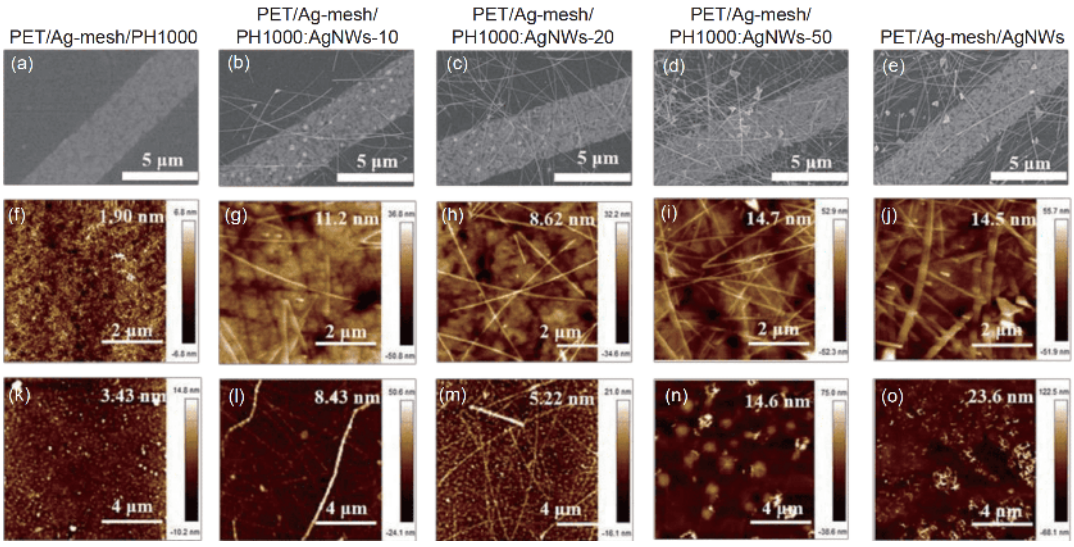

Figure 3 SEM (a–e) and AFM images (f–j) of PET/Ag-mesh/PH1000:AgNWs with various AgNWs weight ratios; (k–o) AFM images of the corresponding flexible electrodes coated with PEIE/AZO (color online).

PH1000 film. Notably, when doping 20 wt% AgNWs, the resulting PET/Ag-mesh/PH1000:AgNWs-20 composite electrode showed the lowest RMS (8.62 nm, Figure 3(h)), which is even lower than that of PH1000:AgNWs-10. The RMS can be further reduced to 5.22 nm after coating with PEIE/AZO ETL. The significantly improved morphology could be attributed to well-formed AgNWs network, which can restrain random distribution of AgNWs at a 20 wt%. In comparison, both the high- and low-content AgNWs would enhance their random distribution. Particularly for the PET/Ag-mesh/PH1000:AgNWs-50 and PET/Ag-mesh/AgNWs, some weak aggregation and randomly unconnected wire-wire contacts were even observed. We also noted that the long-time thermal annealing process could further deteriorate the morphology of flexible electrode, giving a high RMS of 23.5 nm (Figure S2). This behavior led to a rough surface after coating with PEIE/AZO (Figure 3(o)).

3.3 Photovoltaic performance

To evaluate the photovoltaic properties of these flexible composite electrodes, the devices with a structure of PET/Ag-mesh/PH1000 with or without Ag-NWs/PEIE/AZO/PBDB-T-2F:IT-4F/MoO_3/Al (Figure 1(a)) were fabricated, where PEIE/AZO was selected as ETL. The corresponding device parameters are listed in Table 1. Figure 4(a) shows the *J-V* characteristics of flexible OSCs based on PET/Ag-mesh/PH1000:AgNWs electrodes under different AgNWs doping ratios. We can find that the AgNWs doped in PH1000 has a significant influence on the performance of flexible OSCs. The control device based on PET/Ag-mesh/PH1000 electrode exhibited a PCE of 11.12% with an open circuit voltage (V_{oc}) of 0.787 V, a short-circuit current density (J_{sc}) of 20.52 mA/cm^2 and a fill factor (FF) of 68.85%. After doping 10-wt%-AgNWs in PH1000, the PET/Ag-mesh/PH1000:AgNWs-10-based flexible OSCs showed a slightly increased PCE of 11.33%. When further increasing the AgNWs ratio, a PCE over 12% can be reached. To the best of our knowledge, the 12.07% PCE is the highest reported value for the flexible ITO-free OSCs. However, we noted that the J_{sc} value was only slightly increased (~2%), although the flexible electrode doping with 20 wt% AgNWs showed an approximately 5% enhanced transmittance compared with that without doping AgNWs. This mismatch was probably caused by the small deviation of active layer thickness due to the various roughness of flexible electrodes. Instead, the enhanced PCE

Table 1 Photovoltaic parameters of flexible OSCs with the structure of PET/Ag-mesh/PH1000:Ag-NWs/PEIE/AZO/PBDB-T-2F:IT-4F/MoO_3/Al under the illumination of AM 1.5G (100 mW/cm^2). The average PCE was calculated from 10 devices

Electrode	V_{oc} (V)	J_{sc} (mA/cm^2)	FF (%)	PCE (%)
PET/Ag-mesh/PH1000	0.787	20.52	68.85	11.12 (10.67±0.29)
PET/Ag-mesh/PH1000:AgNWs-10	0.803	20.65	68.31	11.33 (10.93±0.26)
PET/Ag-mesh/PH1000:AgNWs-20	0.826	20.90	69.87	12.07 (11.82±0.26)
PET/Ag-mesh/PH1000:AgNWs-50	0.762	21.24	54.88	8.88 (7.09±1.19)
PET/Ag-mesh/AgNWs	0.731	21.25	55.60	8.64 (7.52±0.81)
Glass/ITO	0.835	21.23	73.04	12.94

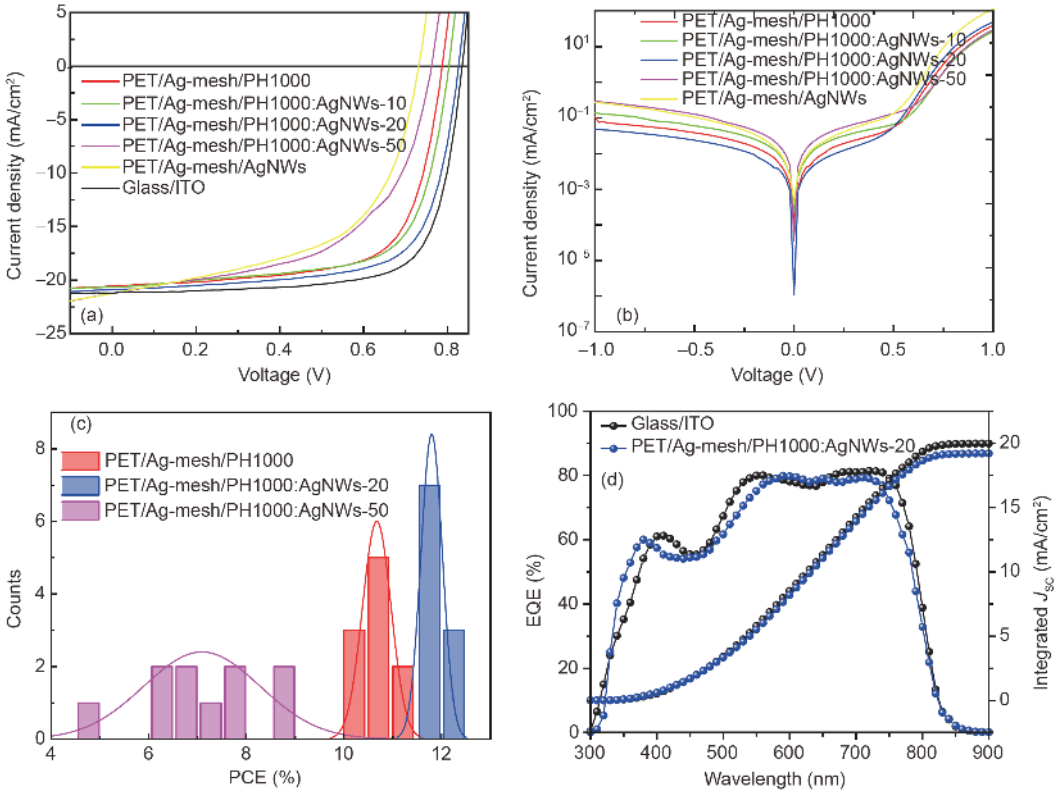

Figure 4 Light (a) and dark (b) *J-V* characteristics of the flexible OSCs based on PET/Ag-mesh/PH1000:AgNWs flexible electrodes with various AgNWs doping ratios; (c) PCE histogram of flexible OSCs; (d) EQE spectra of the flexible solar cells based on PET/Ag-mesh/PH1000:AgNWs-20 electrodes and Glass/ITO electrodes (color online).

mainly originated from the increased V_{oc} from 0.787 to 0.826 V, which is attributed to the decreased work function of AgNWs doped PH1000, and thus is favorable to form ohmic contact with ETL [43]. However, for the electrodes with high content of AgNWs (PET/Ag-mesh/PH1000:AgNWs-50 and PET/Ag-mesh/AgNWs), their device PCEs were dramatically decreased to 8.88% and 8.64% owing to the reduced V_{oc} and FF. These deteriorated photovoltaic properties were probably caused by the large leakage current and lower rectification ratio (Figure 4(b)) originating from the high RMS of flexible electrodes that are likely to induce shunting channels through the active layer [44]. Figure 4(c) illustrates the PCE histogram of the flexible OSCs, the devices based on high-content-AgNWs electrodes, e.g. PET/Ag-mesh/PH1000:AgNWs-50%, showed an extremely poor device reproducibility due to the high roughness of flexible electrode. While, the PET/Ag-mesh/PH1000:AgNWs-20% electrode with smooth surface, low sheet resistance and high transmittance provide a feasibility to fabricate flexible OSCs toward high efficiency accompanying with high reproducibility (standard deviation of 0.22). Figure 4(d) shows the external quantum efficiency (EQE) spectra of the OSCs based on PET/Ag-mesh/PH1000:AgNWs-20 electrodes and Glass/ITO electrodes, respectively. The integrated current densities are 19.22 mA/cm^2 for flexible device and 19.98 mA/cm^2 for rigid device, which are well consistent with the results obtained from *J-V* curves. The slightly higher deviation of flexible OSCs may be attributed to the curved PET surface caused by thermal annealing process.

To gain more insight into the AgNWs doping effect on the charge dynamic of flexible OSCs, we carried out PL, carrier transport and collection measurements. As shown in Figure 5 (a), the active layer deposited on PET/Ag-mesh/PH1000:AgNWs-20%/PEIE/AZO exhibited a lower PL intensity (excited at 555 nm) than that of PET/Ag-mesh/PH1000/PEIE/AZO, indicating a better carrier extracting ability for the electrode containing 20 wt% AgNWs. The dependence of V_{oc} on light intensity measurement, giving a relationship of $V_{oc} \propto (nkT/q)\ln(P_{light})$, was then used to further evaluate the carrier recombination behavior. The smallest slope of 1.14 kT/q for flexible OSCs suggested that the PBDB-T-2F:IT-4F active layer deposited on high-quality flexible electrode could suppress trap-assisted recombination (Figure 5(b)) [45].

4 Conclusions

In conclusion, we have successfully developed a high-quality composite flexible electrode by combining AgNWs doped

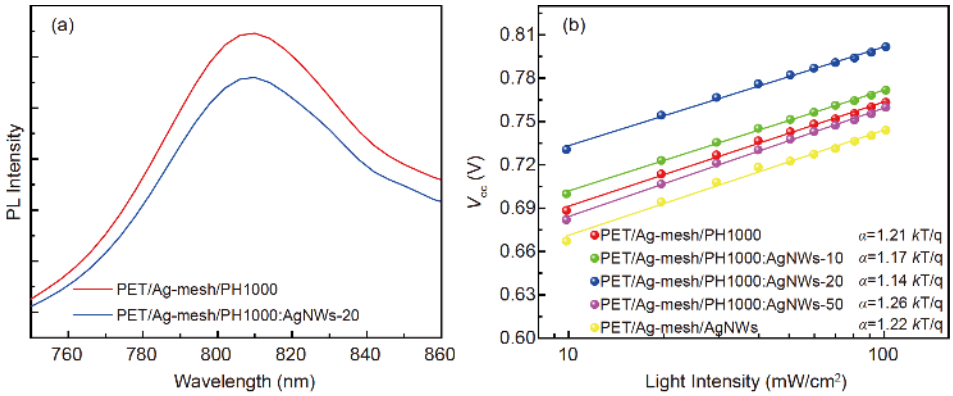

Figure 5 (a) PL spectra of flexible OSCs based on PET/Ag-mesh/PH1000 and PET/Ag-mesh/PH1000:AgNWs-20% electrodes; (b) V_{oc} versus natural logarithm of light intensities fitted by a linear relationship for the various flexible electrodes-based OSCs (color online).

PH1000 with PET/Ag-mesh substrate. By this strategy, both the optical and electronic properties of flexible electrode can be improved. The optimized flexible electrode PET/Ag-mesh/PH1000:AgNWs-20 possesses a low sheet resistance of ~6 Ω/sq and high transmittance of 86% at 550 nm wavelength. The flexible OSCs based on this electrode achieved a record PCE of 12.07% with high reproducibility when selecting PBDB-T-2F:IT-4F as active layers and PEIE/AZO as ETL. It demonstrated that this flexible composite electrode has a good compatibility with the conventional device structure, opening a new direction for designing high-quality flexible electrodes toward high performance OSCs.

Acknowledgements This work was supported by the National Natural Science Foundation of China (51673138, 51820105003, 91633301), the Priority Academic Program Development of Jiangsu Higher Education Institutions, the Jiangsu Provincial Natural Science Foundation (BK20160059), Natural Science Foundation of the Jiangsu Higher Education Institutions of China (16KJB430027), and the National Key Research and Development Program of China (2017YFA0207700).

Conflict of interest The authors declare that they have no conflict of interest.

Supporting information The supporting information is available online at http://chem.scichina.com and http://link.springer.com/journal/11426. The supporting materials are published as submitted, without typesetting or editing. The responsibility for scientific accuracy and content remains entirely with the authors.

1 Chang SY, Cheng P, Li G, Yang Y. *Joule*, 2018, 2: 1039–1054
2 Yu R, Yao H, Hong L, Qin Y, Zhu J, Cui Y, Li S, Hou J. *Nat Commun*, 2018, 9: 4645
3 Sun C, Xia R, Shi H, Yao H, Liu X, Hou J, Huang F, Yip HL, Cao Y. *Joule*, 2018, 2: 1816–1826
4 Zhang S, Ye L, Zhao W, Yang B, Wang Q, Hou J. *Sci China Chem*, 2015, 58: 248–256
5 Kan B, Feng H, Yao H, Chang M, Wan X, Li C, Hou J, Chen Y. *Sci China Chem*, 2018, 61: 1307–1313
6 Chen W, Zhang J, Xu G, Xue R, Li Y, Zhou Y, Hou J, Li Y. *Adv Mater*, 2018, 30: 1800855
7 Bo Z. *Sci China Chem*, 2018, 61: 507–508
8 Li Y, Xu G, Cui C, Li Y. *Adv Energy Mater*, 2018, 8: 1701791
9 Kim T, Kim JH, Kang TE, Lee C, Kang H, Shin M, Wang C, Ma B, Jeong U, Kim TS, Kim BJ. *Nat Commun*, 2015, 6: 8547
10 Li D, Lai WY, Zhang YZ, Huang W. *Adv Mater*, 2018, 30: 1704738
11 Li H, Liu X, Wang W, Lu Y, Huang J, Li J, Xu J, Fan P, Fang J, Song W. *Sol RRL*, 2018, 2: 1800123
12 Hu L, Kim HS, Lee JY, Peumans P, Cui Y. *ACS Nano*, 2010, 4: 2955–2963
13 Seo JH, Hwang I, Um HD, Lee S, Lee K, Park J, Shin H, Kwon TH, Kang SJ, Seo K. *Adv Mater*, 2017, 29: 1701479
14 Ahn BY, Duoss EB, Motala MJ, Guo X, Park SI, Xiong Y, Yoon J, Nuzzo RG, Rogers JA, Lewis JA. *Science*, 2009, 323: 1590–1593
15 Ghosh DS, Chen TL, Pruneri V. *Appl Phys Lett*, 2010, 96: 041109
16 Meng W, Ge R, Li Z, Tong J, Liu T, Zhao Q, Xiong S, Jiang F, Mao L, Zhou Y. *ACS Appl Mater Interfaces*, 2015, 7: 14089–14094
17 Fan X, Xu B, Liu S, Cui C, Wang J, Yan F. *ACS Appl Mater Interfaces*, 2016, 8: 14029–14036
18 Luo Q, Ma H, Hao F, Hou Q, Ren J, Wu L, Yao Z, Zhou Y, Wang N, Jiang K, Lin H, Guo Z. *Adv Funct Mater*, 2017, 27: 1703068
19 Song W, Fan X, Xu B, Yan F, Cui H, Wei Q, Peng R, Hong L, Huang J, Ge Z. *Adv Mater*, 2018, 30: 1800075
20 Ou QD, Xie HJ, Chen JD, Zhou L, Li YQ, Tang JX. *J Mater Chem A*, 2016, 4: 18952–18962
21 Kim J, Park S, Lee S, Ahn H, Joe S, Kim BJ, Son HJ. *Adv Energy Mater*, 2018, 8: 1801601
22 Xu X, Fukuda K, Karki A, Park S, Kimura H, Jinno H, Watanabe N, Yamamoto S, Shimomura S, Kitazawa D, Yokota T, Umezu S, Nguyen TQ, Someya T. *Proc Natl Acad Sci USA*, 2018, 139: 201801187–4594
23 Huang J, Li CZ, Chueh CC, Liu SQ, Yu JS, Jen AKY. *Adv Energy Mater*, 2015, 5: 1500406
24 Heywang G, Jonas F. *Adv Mater*, 1992, 4: 116–118
25 Reyes-Reyes M, Cruz-Cruz I, López-Sandoval R. *J Phys Chem C*, 2010, 114: 20220–20224
26 Zhang W, Zhao B, He Z, Zhao X, Wang H, Yang S, Wu H, Cao Y. *Energy Environ Sci*, 2013, 6: 1956–1964
27 Kim N, Kee S, Lee SH, Lee BH, Kahng YH, Jo YR, Kim BJ, Lee K. *Adv Mater*, 2014, 26: 2268–2272
28 Ouyang J, Chu CW, Chen FC, Xu Q, Yang Y. *Adv Funct Mater*, 2005, 15: 203–208
29 Wang BY, Yoo TH, Lim JW, Sang BI, Lim DS, Choi WK, Hwang DK, Oh YJ. *Small*, 2015, 11: 1905–1911
30 Langley D, Giusti G, Mayousse C, Celle C, Bellet D, Simonato JP. *Nanotechnology*, 2013, 24: 452001
31 Li Y, Meng L, Yang YM, Xu G, Hong Z, Chen Q, You J, Li G, Yang Y, Li Y. *Nat Commun*, 2016, 7: 10214
32 Xu G, Xue R, Chen W, Zhang J, Zhang M, Chen H, Cui C, Li H, Li Y,

Li Y. *Adv Energy Mater*, 2018, 8: 1703054
33 Zhang J, Xue R, Xu G, Chen W, Bian GQ, Wei C, Li Y, Li Y. *Adv Funct Mater*, 2018, 28: 1705847
34 Zhang M, Guo X, Ma W, Ade H, Hou J. *Adv Mater*, 2015, 27: 4655–4660
35 Zhao W, Li S, Yao H, Zhang S, Zhang Y, Yang B, Hou J. *J Am Chem Soc*, 2017, 139: 7148–7151
36 Liu X, Li X, Li Y, Song C, Zhu L, Zhang W, Wang HQ, Fang J. *Adv Mater*, 2016, 28: 7405–7412
37 Li P, Wang G, Cai L, Ding B, Zhou D, Hu Y, Zhang Y, Xiang J, Wan K, Chen L, Alameh K, Song Q. *Phys Chem Chem Phys*, 2014, 16: 23792–23799
38 Jin WY, Ginting RT, Jin SH, Kang JW. *J Mater Chem A*, 2016, 4: 3784–3791
39 Kang SB, Noh YJ, Na SI, Kim HK. *Sol Energy Mater Sol Cells*, 2014, 122: 152–157
40 Lee J, Lee P, Lee HB, Hong S, Lee I, Yeo J, Lee SS, Kim TS, Lee D, Ko SH. *Adv Funct Mater*, 2013, 23: 4171–4176
41 Leem DS, Edwards A, Faist M, Nelson J, Bradley DDC, de Mello JC. *Adv Mater*, 2011, 23: 4371–4375
42 Alvarez MM, Khoury JT, Schaaff TG, Shafigullin MN, Vezmar I, Whetten RL. *J Phys Chem B*, 1997, 101: 3706–3712
43 Zhou H, Wang Y, Zhang J, Yu Z, Li Y, Tan L, Chen Y. *J Mater Chem C*, 2018, 6: 312–319
44 Liu X, Tan X, Liu Z, Ye H, Sun B, Shi T, Tang Z, Liao G. *Nano Energy*, 2018, 56: 184–195
45 Zhang L, Xu X, Lin B, Zhao H, Li T, Xin J, Bi Z, Qiu G, Guo S, Zhou K, Zhan X, Ma W. *Adv Mater*, 2018, 30: 1805041